

ISSN: 2576-8840





# Theoretical Investigation on Palladium-Catalyzed Spirocyclopropanation of $\pi$ -Allylpalladium 1,4-Dipole with *gem*-Difluoroalkene or via 1,4-Addition-Induced Dearomatization of 5-Alkenylthiazolone with 2-Bromomalonate

\*Corresponding author: Nan Lu, College of Chemistry and Material Science, Shandong Agricultural University, Taian 271018, P. R. China

**Nan Lu\* and Chengxia Miao**

College of Chemistry and Material Science, Shandong Agricultural University, P. R. China

Submission:  July 13, 2024

Published:  July 18, 2024

Volume 20 - Issue 3

**How to cite this article:** Nan Lu\* and Chengxia Miao. Theoretical Investigation on Palladium-Catalyzed Spirocyclopropanation of  $\pi$ -Allylpalladium 1,4-Dipole with *gem*-Difluoroalkene or via 1,4-Addition-Induced Dearomatization of 5-Alkenylthiazolone with 2-Bromomalonate. Res Dev Material Sci. 20(3). RDMS. 000988. 2024.

DOI: [10.31031/RDMS.2024.20.000988](https://doi.org/10.31031/RDMS.2024.20.000988)

**Copyright**© Nan Lu, This article is distributed under the terms of the Creative Commons Attribution 4.0 International License, which permits unrestricted use and redistribution provided that the original author and source are credited.

## Abstract

The mechanism is investigated for Pd(0)-catalyzed spirocyclopropanation of  $\pi$ -allylpalladium 1,4-dipole with *gem*-difluoroalkene and 1,4-addition-induced dearomatization of 5-alkenylthiazolone with 2-bromomalonate. The  $\pi$ -allylpalladium 1,4-zwitterionic species was afforded by oxidative addition and rate-limiting decarboxylation. Then nucleophilic addition of anionic oxygen to *gem*-difluorinated carbon generated zwitterionic intermediate with dual Pd- $\pi$  coordination. The intramolecular spirocyclization underwent through attack of anionic carbon to central carbon of  $\pi$ -allylpalladium giving palladacyclobutane, the reductive elimination of which yielded oxa/azaspiro [2.4]-heptane and Pd(0). The carbonyl of 5-alkenylthiazolone was activated by quaternary ammonium with enhanced electrophilicity of C-C double bond, which was attacked by carbanion of deprotonated bromomalonate in Michael 1,4-addition forming aromatized enolate. Subsequently, the rate-limiting intramolecular  $S_N2$  nucleophilic substitution took place affording dearomatized ring closure product spirocyclopropylthiazole. The positive solvation effect is suggested by decreased absolute and activation energies in solution compared with in gas. These results are supported by Multiwfn analysis on FMO composition of specific TSs, and MBO value of vital bonding, breaking.

**Keywords:** Spirocyclopropanation; 1,4-addition; Dearomatization; 5-alkenylthiazolone;  $\pi$ -allylpalladium 1,4-dipole

## Introduction

As privileged member of pharmaceutical and bioactive molecules, oxa/azaspiro[2.4]-heptanes are significant spirocyclic skeletons. Therefore, the synthetic method was attractive in organic synthesis [1,2]. In the aspect of cyclopropanation based on  $\pi$ -allylpalladium chemistry, much progress has been achieved in recent years. Hou contributed to enantioselective cyclopropanation of nitriles with mono substituted allyl carbonates enabled by N-heterocyclic carbene ligand [3]. Liu employed asymmetric decarboxylative [3 + 2] cycloaddition for diastereo- and enantioselective synthesis of spiro[2.4]heptanes applicable for electron-deficient olefins, isocyanates, and aldehydes [4]. Trost reported Pd-

catalyzed spirocyclopropanation of acyclic allyl alcohol esters with nitroalkenes as Michael receptors [5]. The *gem*-difluoroalkenes are powerful substrates as vital fluorine sources in many [3 + 2] and [4 + 2] annulations [6-9]. The palladium-catalyzed formal [3 + 2] cycloaddition could deliver chiral 2,2-difluoro-3-aryl-4-vinyltetrahydrofurans with vinyl epoxides and vinyl ethylene carbonates (VECs) as  $\pi$ -allylpalladium precursors [10].

The conformational rigidity and intrinsic complexity of spirocyclic compounds provide advantages for them in drug discovery and pharmaceuticals [11-13], among which the spirocyclopropane and thiazole are privileged and attractive skeletons as biologically active natural products [14,15]. Owing to the ability of linking receptors or enzymes, they often function in fields of pharmacophores such as chiral 4-acyloxythiazole obtained from bifunctional squaramide-catalysed asymmetric Michael/hemiketalization/retro-aldol reaction of unsaturated thiazolones with  $\alpha$ -nitroketones [16] and novel pyridine-thiazolidinone as anticancer agents [17]. In fruitful area of adding functional diversity, the fused thiazole derivatives are mostly focused on with strong driving force of aromatization. Yang reported organocatalytic inverse-electron-demand Diels-Alder reaction between  $\beta,\gamma$ -unsaturated carbonyl compounds and 5-alkenyl thiazolones [18]. However, dearomatized spirothiazole products are relatively difficult to obtain. Only Mei developed asymmetric [3 + 2] annulation of isatin-derived MBH carbonates and 5-alkenylthiazol-4(5H)-ones with catalyst-controlled switchable diastereoselectivity [19]. With readily available C1 synthons, bromomalonate is attractive and exhibiting good nucleophilicity in construction of cyclopropanes under basic condition [20].

Beller realized *gem*-fluorinated spirocycle via palladium-catalyzed cascade reaction of *gem*-difluoroallyl ammonium salt with *o*-halophenol including  $S_N2'$  substitution, Heck reaction, C-H activation, reductive elimination or alkyne insertion [21]. In this context, a breakthrough was Xu's palladium-catalyzed spirocyclopropanation of *gem*-difluoroalkene with  $\pi$ -allylpalladium 1,4-dipole [22]. In addition, great progress appeared for spirocyclization reaction between bromomalonate and benzofuran-derived azadiene/oxadiene or pyrazole-derived oxadiene [23,24]. After this, the reactivity of 5-alkenylthiazolone was explored under basic condition to prepare spirocyclopropane [25]. Although skeletons of oxa/azaspiro[2.4]-heptane were obtained with various functional group, many problems still puzzled and there was no report about detailed mechanistic study explaining Pd(0)-catalyzed spirocyclopropanation. How the vital  $\pi$ -allylpalladium zwitterionic intermediate is formed via nucleophilic addition? How Pd(0) species influence the decarboxylation of methylenetriethylamine carbonate? What is the process for Michael 1,4-addition induced dearomatization strategy? How the excellent diastereoselectivity is controlled for spirocyclopropylthiazole product bearing two consecutive quaternary centers? To solve these questions in

experiment, an in-depth theoretical study was necessary for this strategy focusing on the competition between spirocyclopropanation and  $\beta$ -F elimination.

## Computational Details

The geometry optimizations were performed at the B3LYP/BSI level with the Gaussian 09 package [26,27]. The mixed basis set of LanL2DZ for Pd and 6-31G(d) for non-metal atoms [28-32] was denoted as BSI. Different singlet and multiplet states were clarified with B3LYP and ROB3LYP approaches including Becke's three-parameter hybrid functional combined with Lee-Yang-Parr correction for correlation [33-39]. The nature of each structure was verified by performing harmonic vibrational frequency calculations. Intrinsic Reaction Coordinate (IRC) calculations were examined to confirm the right connections among key transition-states and corresponding reactants and products. Harmonic frequency calculations were carried out at the B3LYP/BSI level to gain Zero-Point Vibrational Energy (ZPVE) and thermodynamic corrections at 333, 323K and 1 atm for each structure in THF, acetonitrile. The solvation-corrected free energies were obtained at the B3LYP/6-311++G(d,p) (LanL2DZ for Pd) level by using integral equation formalism polarizable continuum model (IEFPCM) in Truhlar's "density" solvation model [40-42] on the B3LYP/BSI-optimized geometries.

As an efficient method obtaining bond and lone pair of a molecule from modern ab initio wave functions, NBO procedure was performed with Natural bond orbital (NBO3.1) to characterize electronic properties and bonding orbital interactions [43,44]. The wave function analysis was provided using Multiwfn\_3.7\_dev package [45] including research on Frontier Molecular Orbital (FMO) and Mayer Bond Order (MBO).

## Results and Discussion

The mechanism was explored for Pd(0)-catalyzed spirocyclopropanation of  $\pi$ -allylpalladium 1,4-dipole 1 with *gem*-difluoroalkene 2 leading to *gem*-difluorinated oxa/azaspiro[2.4]-heptane 3 and 1,4-addition-induced dearomatization of 5-alkenylthiazolone 5 with 2-bromomalonate 6 giving spirocyclopropylthiazole 7 (Figure 1). On one hand, illustrated by black arrow of Figure 2a, initially the  $\pi$ -allylpalladium 1,4-zwitterionic species was given by oxidative addition of 1 to Pd(0) and decarboxylation. Then via nucleophilic addition, the electrophilic *gem*-difluorinated carbon atom of 2 was attacked by anionic oxygen forming zwitterionic intermediate B, which underwent intramolecular spirocyclization through the attack of anionic carbon to central carbon of  $\pi$ -allylpalladium giving palladacyclobutane C with five-membered ring. The product 3 was finally obtained with three-membered ring via reductive elimination of C as well as the regenerated Pd(0) species. Added by HF, the competitive  $\beta$ -F elimination also existed from 2 yielding trifluoromethyl 4 as by-product (blue arrow of Figure 2a).

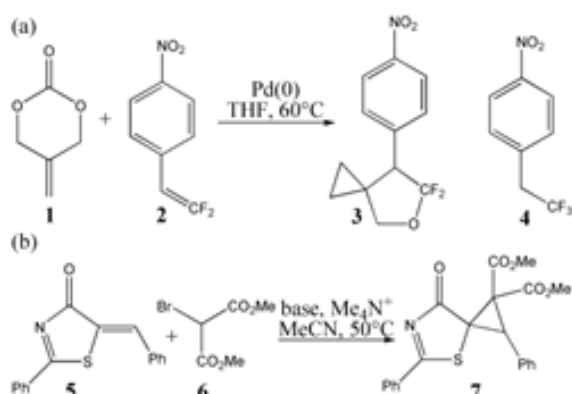


**Figure 1:** (a) Pd(0)-catalyzed spirocyclopropanation of  $\pi$ -allylpalladium 1,4-dipole **1** with *gem*-difluoroalkene **2** leading to *gem*-difluorinated oxa/azaspiro[2.4]-heptane **3**, (b) 1,4-addition-induced dearomatization of 5-alkenylthiazolone **5** with 2-bromomalonate **6** giving spirocyclopropylthiazole **7**.

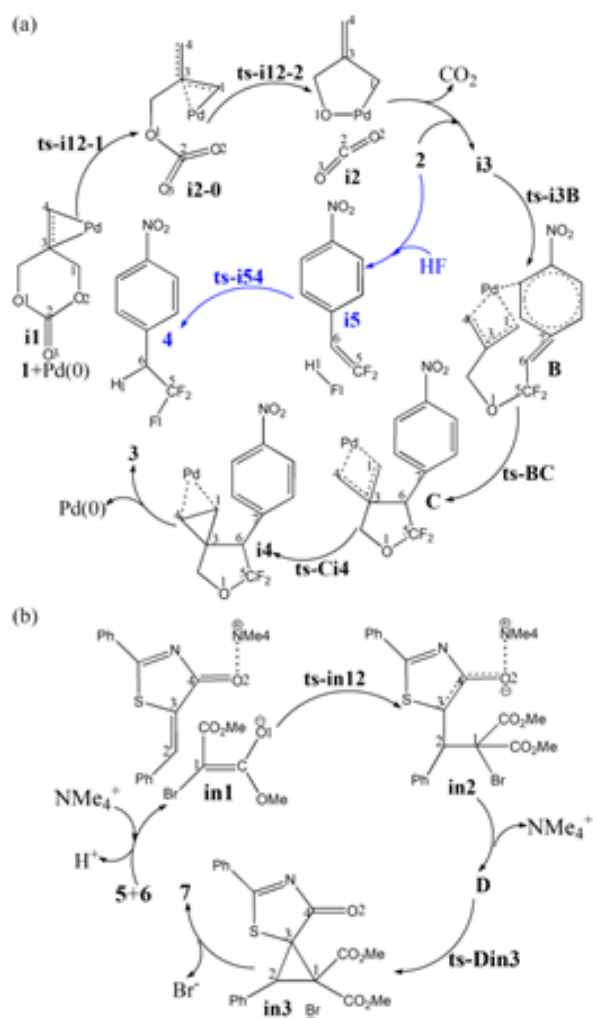


**Figure 1:** Proposed reaction mechanism of (a) Pd(0)-catalyzed spirocyclopropanation of **1** with **2** leading to **3**, (b) 1,4-addition-induced dearomatization of **5** with **6** giving **7**. TS is named according to the two intermediates it connects.

On the other hand (black arrow of Figure 2b), carbanion was furnished for deprotonated bromomalonate **6**. In the meantime, the carbonyl of **5** was activated by quaternary ammonium Me<sub>4</sub>N<sup>+</sup> with enhanced electrophilicity of C-C double bond, which was attacked by carbanion in Michael 1,4-addition forming aromatized enolate intermediate **D** after removal of Me<sub>4</sub>N<sup>+</sup>. Then an intramolecular S<sub>N</sub>2 nucleophilic substitution took place affording dearomatized ring closure product **7** followed by the release of Br<sup>-</sup>. The schematic structures of optimized TSs in Figure 2 were listed by Figure 3. The activation energy was shown in Table 1 for all steps. Supplementary Table 2, Table 3 provided the relative energies of all stationary points. According to experiment, the Gibbs free energies in THF, acetonitrile solution phase are discussed here.

**Table 1:** The activation energy (in kcal mol<sup>-1</sup>) of all reactions in gas and solvent.

TS	$\Delta G_{\text{gas}}^{\ddagger}$	$\Delta G_{\text{sol}}^{\ddagger}$
ts-i12-1	31.2	24.8
ts-i12-2	16.5	12.1
ts-i3B	18.8	17.5
ts-BC	27.0	20.8
ts-Ci4	17.1	14.8
ts-i54	35.8	28.5
ts-in12	8.1	6.7
ts-Din3	9.6	8.5

**Table 2:** Calculated relative energies (all in kcal mol<sup>-1</sup>, relative to isolated species) for the ZPE-corrected Gibbs free energies ( $\Delta G_{\text{gas}}$ ), Gibbs free energies for all species in solution phase ( $\Delta G_{\text{sol}}$ ) at 333, 323K by B3LYP/6-311++G(d,p)//B3LYP/6-31G(d) method and difference between absolute energy.

Species	$\Delta G_{\text{gas}}$	$\Delta G_{\text{sol(THF)}}$
1+pd0	0.00	0.00
i1	-136.13	-132.59
ts-i12-1	-104.93	-107.79
i2-0	-127.45	-124.66
ts-i12-2	-110.94	-112.56
i2	-137.10	-138.69
1+pd0-co2	0.00	0.00
A	-75.77	-73.26
1+pd0-co2+2	0.00	0.00
i3	-255.51	-264.25
ts-i3B	-236.70	-246.72
B	-261.74	-267.55
ts-BC	-234.73	-246.79
C	-287.38	-290.35
ts-Ci4	-270.29	-275.58
i4	-293.39	-287.15
1-co2+2	0.00	0.00
3	-34.45	-40.57
hf+2	0.00	0.00

i5	-0.27	-2.25
ts-i54	35.49	26.23
4	-24.35	-30.99
Species	$\Delta G_{\text{gas}}$	$\Delta G_{\text{sol(MeCN)}}$
5+6-h+nme4	0.00	0.00
in1	-19.06	-22.54
ts-in12	-10.98	-15.81
in2	-29.35	-36.70
5+6-h	0.00	0.00
D	-15.37	-19.92
ts-Din3	-5.77	-11.44
in3	-28.51	-38.06
5+6-h-br	0.00	0.00
7	-4.81	-9.66

**Table 3:** The activation energy (local barrier) (in kcal mol<sup>-1</sup>) of all reactions in the gas, solution phase calculated with B3LYP/6-311++G(d,p)//B3LYP/6-31G(d) method.

TS	$\Delta G_{\text{gas}}^{\ddagger}$	$\Delta G_{\text{sol}}^{\ddagger}$
ts-i12-1 (302i)	31.2	24.8
ts-i12-2 (188i)	16.5	12.1
ts-i3B (312i)	18.8	17.5
ts-BC (209i)	27.0	20.8
ts-Ci4 (134i)	17.1	14.8
ts-i54 (1703i)	35.8	28.5
ts-in12 (194i)	8.1	6.7
ts-Din3 (251i)	9.6	8.5

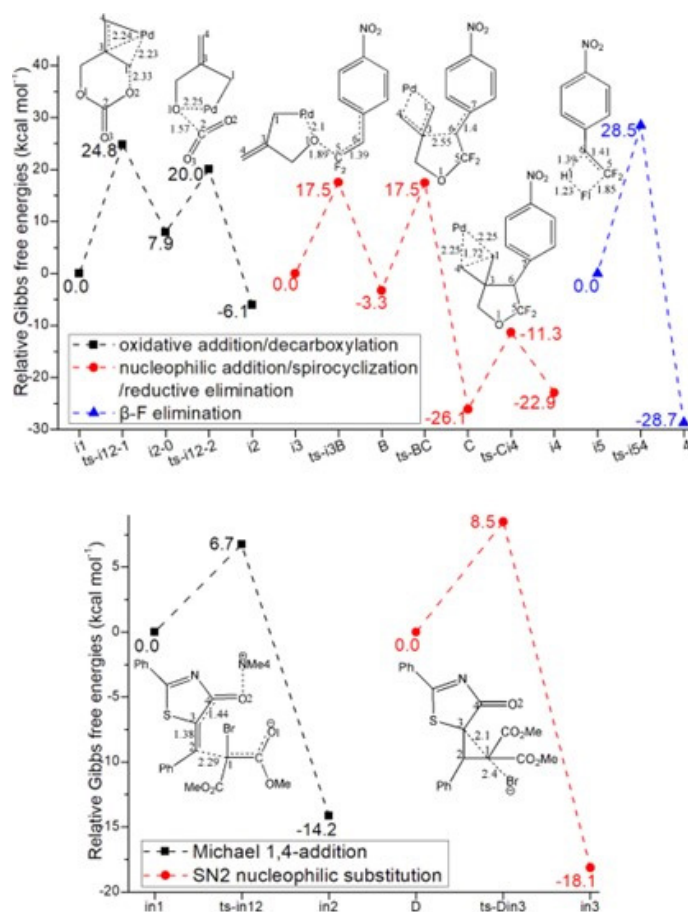


**Figure 3:** Relative Gibbs free energy profile in solvent phase starting from complex (a) **i1**, **i3**, **i5** (b) **in1**, **D** (Bond lengths of optimized TSs in Å).

### Oxidative addition, decarboxylation

Initially the oxidative addition of **1** to Pd(0) gives a stable complex denoted as **i1**, which is characterized by the coordination of methylene  $\pi$  electron to Pd with Pd-C3 and Pd-C4 bond. The following decarboxylation requires two steps. First C1-O2 is cleaved via ts-i12-1 as step 1 with the activation energy of

24.8kcal mol<sup>-1</sup> relative to the starting point **i1** endothermic by 7.9kcal mol<sup>-1</sup> (black dash line of Figure 3a). The transition vector not only includes the dissociation of C1...O2 but the coordinated shifting from Pd-C3 to Pd-C1 with Pd-C4 still bonded (2.33, 2.24, 2.23Å) (Figure 4a). There are strong Pd-C1 single bond and weak Pd-C3 in resultant **i2-0**.



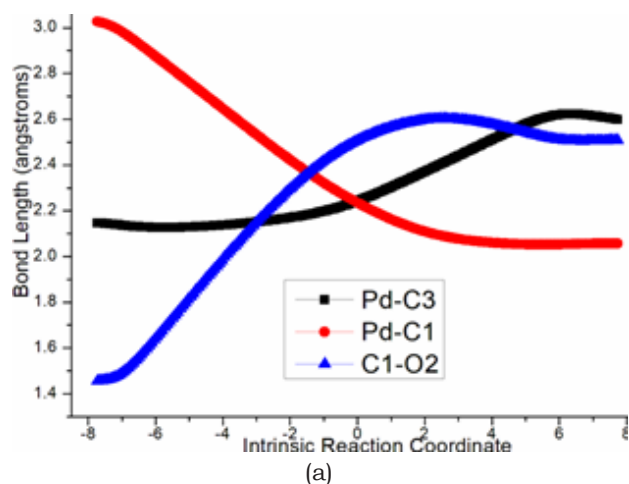


**Figure 4(a):** Evolution of bond lengths along the IRC for (a) ts-i12-1

In step 2, decarboxylation is completed via the disruption of O1-C2 bond via ts-i12-2 with activation energy of 12.1 kcal mol<sup>-1</sup> exothermic by -6.1 kcal mol<sup>-1</sup> leading to i2. The transition vector corresponds to the approaching of Pd to O1 and the resulting elongation of O1...C2 (2.25, 1.57 Å) (Figure 4b). Besides formal CO<sub>2</sub> molecule, the π-allylpalladium 1,4-zwitterionic species is located as stable five-membered ring with Pd-C1 and Pd-O1 single bond. It is rational for positive Pd linked with negative O1, which is relation flexible in following process.

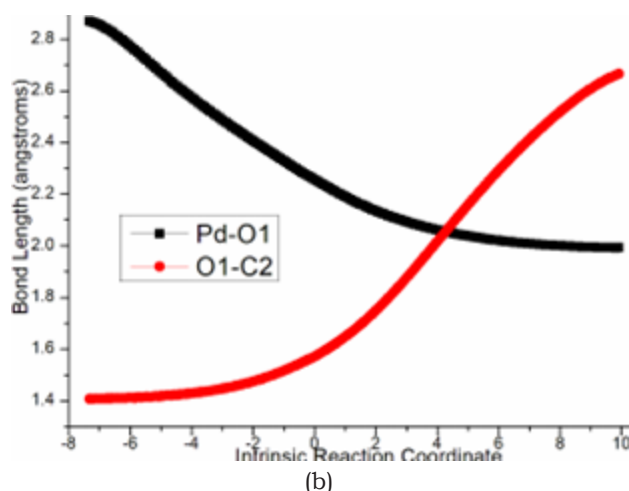


**Figure 4(b):** Evolution of bond lengths along the IRC for (b) ts-i12-2

### Nucleophilic addition, intramolecular spirocyclization, reductive elimination

After the removal of CO<sub>2</sub> from i2, the addition of 2 forms complex i3 as starting point of the following three steps (red dash line of Figure 3a). The nucleophilic addition takes place via ts-i3B in step 3 with activation energy of 17.5 kcal mol<sup>-1</sup> forming zwitterionic intermediate B exothermic by -3.3 kcal mol<sup>-1</sup>. The transition vector suggests the atomic motion composed of O1 leaving from Pd and closing to C5 in the meantime as well as lagged stretching of C5-C6 from double to single (2.10, 1.89, 1.39 Å) (Figure 4c). This

is according to the attack from anionic oxygen O1 to electrophilic *gem*-difluorinated carbon atom C5 prompted by Pd(0) readily accessible. As remarkable activation, Pd-π coordination exists both from methylenetrimesitylene C1-C3-C4 of 1 and benzene ring of 2.

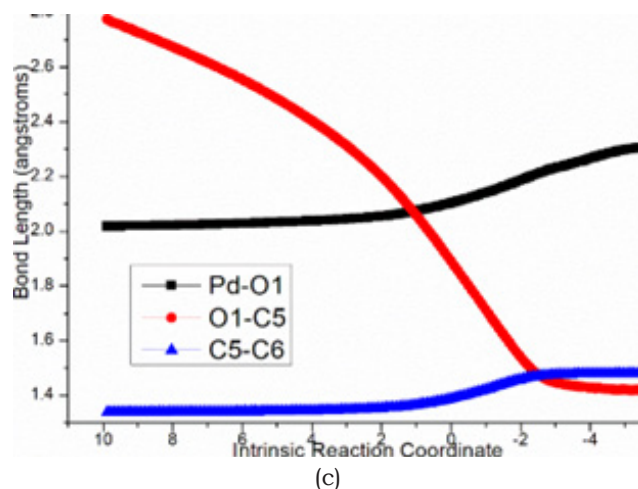


**Figure 4(c):** Evolution of bond lengths along the IRC for (c) ts-i3B

Afterward, B undergoes intramolecular spirocyclization via ts-BC with activation energy of 20.8 kcal mol<sup>-1</sup> in step 4 continuously exothermic by -26.1 kcal mol<sup>-1</sup> generating key palladacyclobutane C with five-membered ring. Here the ring closing is achieved through attack of anionic carbon C6 to central positive carbon C3 of π-allylpalladium. The transition vector is about C6...C3 bonding and C6-C7 elongation from double bond to single (Figure 4d).

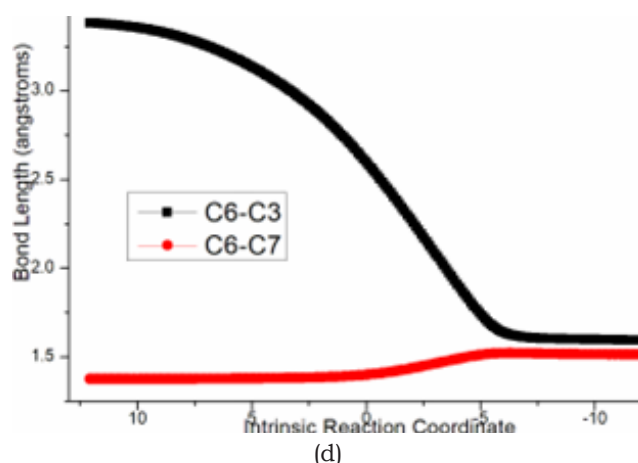


**Figure 4(d):** Evolution of bond lengths along the IRC for (d) ts-BC

At last, the reductive elimination of C proceeds via ts-Ci4 with activation energy of 14.8 kcal mol<sup>-1</sup> exothermic by -22.9 kcal mol<sup>-1</sup> as step 5 producing i4, which is the complex binding desired product 3 and the regenerated Pd(0) species. Once Pd(0) is squeezed from palladacyclobutane, three-membered ring of cyclopropane is finally obtained with C1-C4 bond. This can be illustrated in detail by the transition vector, which includes simultaneous extension of Pd...C1, Pd...C4 and concerted closing of C1...C4 (2.25, 2.25, 1.72 Å) (Figure 4e).

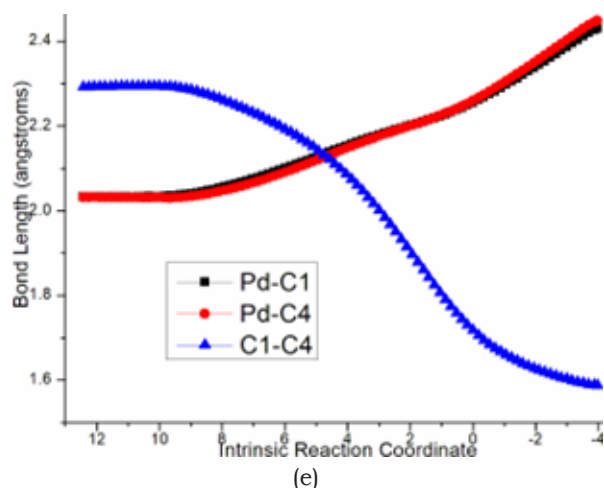


**Figure 4(e):** Evolution of bond lengths along the IRC for (e) ts-Ci4

Ultimately, the first step of decarboxylation is determined to be rate-limiting for Pd(0)-catalyzed spirocyclopropanation. The mediate barrier and heat release confirm this favorable strategy under the assistance of Pd(0) especially considering the experiment temperature of 60 °C. To highlight the idea of feasibility for changes in electron density and not molecular orbital interactions are responsible of the reactivity of organic molecules, quantum

chemical tool Multiwfn was applied to analyze of electron density such as MBO results of bonding atoms and contribution of atomic orbital to HOMO of typical TSs (Table 4, Figure 5). These results all confirm the above analysis.

**Table 4:** Mayer bond order (MBO) of typical TSs.

	Pd...C3	Pd...C1	C1...O2	
ts-i12-1	0.33	0.58	0.17	
	Pd...C1	Pd...O1	O1...C2	
ts-i12-2	0.90	0.33	0.35	
	Pd...O1	O1...C5	C5...C6	
ts-i3B	0.51	0.39	1.37	
	C6...C3	C6...C7		
ts-BC	0.34	1.35		
	Pd...C1	Pd...C4	C1...C4	
ts-Ci4	0.41	0.41	0.66	
	F1...H1	H1...C6	F1...C5	C5...C6
ts-i54	0.34	0.40	0.39	1.25
	C1...C2	C2...C3	C3...C4	
ts-in12	0.30	1.39	1.15	
	C3...C4	C3...C1	C1...Br	
ts-Din3	1.13	0.38	0.49	

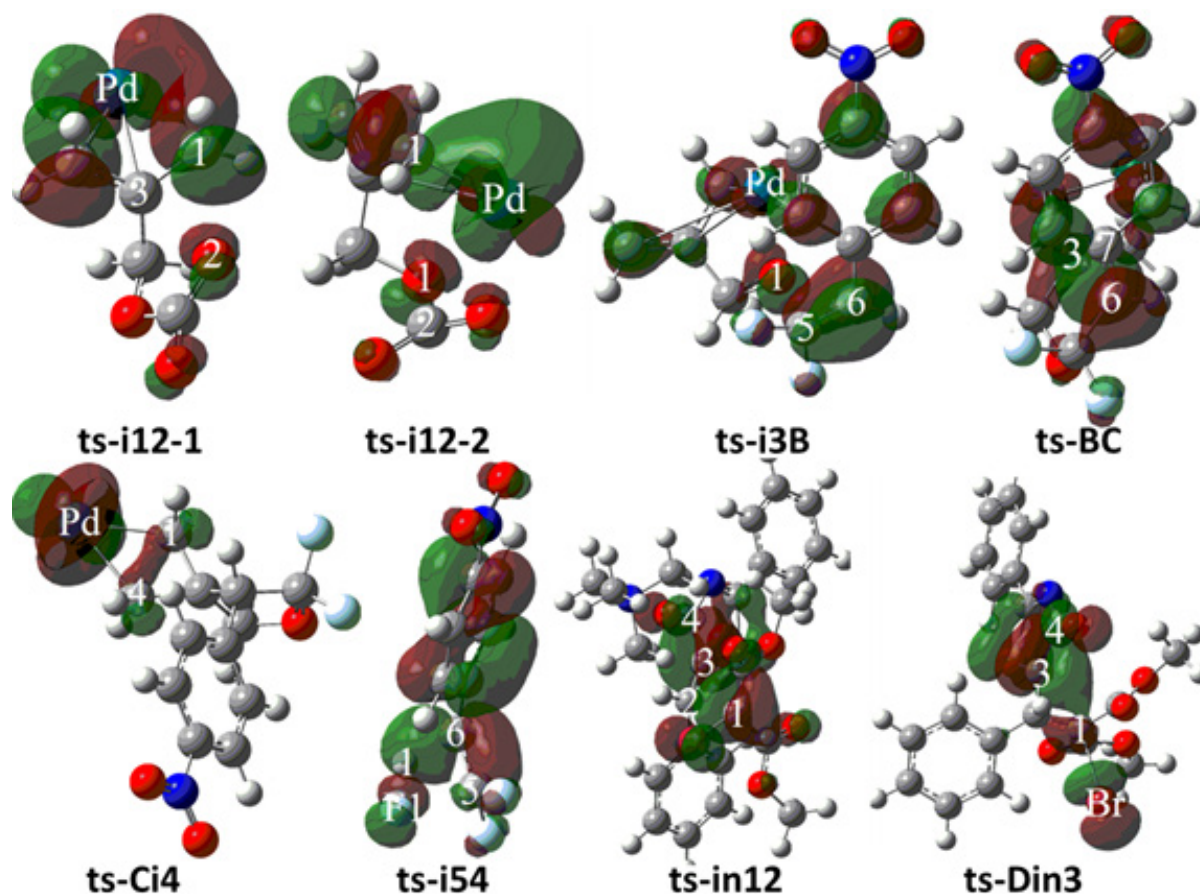


**Figure 5:** Highest Occupied Molecular Orbital (HOMO) of typical TSs. Different colors are used to identify the phase of the wave functions.

### $\beta$ -F elimination, Michael 1,4-addition, intramolecular $S_N2$ nucleophilic substitution

To investigate the competitive  $\beta$ -F elimination, the attack of F-released from specific structure of B was modeled by an additional HF to 2 located as initial i5 (blue dash line of Figure 3a). The alkylation occurs via ts-i54 yielding trifluoromethyl 4 as by-product. The activation energy of this competitive step 6 is 28.5 kcal mol<sup>-1</sup> exothermic by -28.7 kcal mol<sup>-1</sup> relative to i5. Seen from the detailed motion demonstrated by its transition vector, the split of HF gives H1, F1 atom bonded to C6, C5 separately accompanied by C5-C6 double bond extending to single (1.23, 1.39, 1.85, 1.41 Å) (Figure 4f). Although  $\beta$ -F elimination is available in thermodynamics, the higher barrier without Pd(0) verifies its disadvantage compared with the above major spirocyclopropanation. This outcome agrees well with the side reaction of  $\beta$ -F elimination and Pd(0) function in experiment.

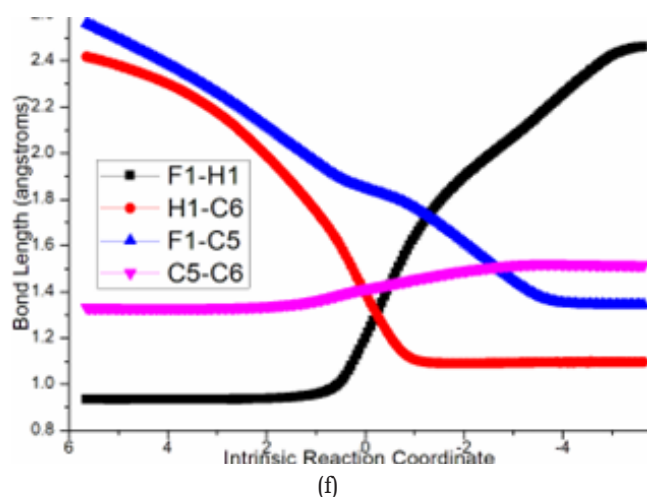


**Figure 4(f):** Evolution of bond lengths along the IRC for (f) ts-i54

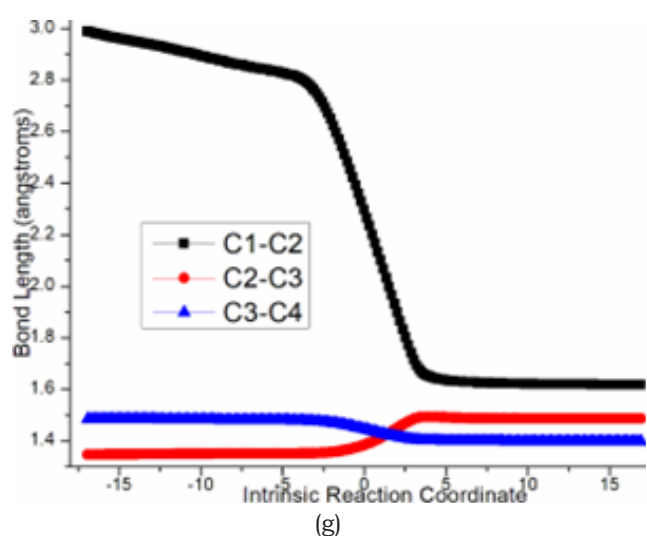


**Figure 4(g):** Evolution of bond lengths along the IRC for (g) ts-in12

On the other, for another spirocyclopropanation of 5 with 6, the real functioned cation of catalyst was selected as quaternary

ammonium Me<sub>4</sub>N<sup>+</sup> and the simple deprotonation of 6 by inorganic base was not considered here. The initial complex in1 was located between carbanion furnished from 6 and 5 activated by Me<sub>4</sub>N<sup>+</sup>, from which Michael 1,4-addition took place via ts-in12 in step 1 with a barrier of 6.7 kcal mol<sup>-1</sup> exothermic by -14.2 kcal mol<sup>-1</sup> delivering in2 (black dash line of Figure 3b). The electrophilicity of C2-C3 double bond was enhanced as a result of carbonyl O2 activated by Me<sub>4</sub>N<sup>+</sup> for 5, which was easily attacked by carbanion C1 of 6. The transition vector corresponds to obvious nucleophilic linkage from C1 to C2, cooperated C2-C3 stretching from double to single and strengthened C3-C4 (2.29, 1.38, 1.44 Å) (Figure 4g). Much negative charge concentrated on O<sub>2</sub> makes in2 rather stable bonded to Me<sub>4</sub>N<sup>+</sup>.

Subsequently, the negative charge shifting from carbonyl O2 to C3 increased the nucleophilicity of C3 while weakened the electrostatic interaction with Me<sub>4</sub>N<sup>+</sup> in the meantime. With the removal of Me<sub>4</sub>N<sup>+</sup>, the optimized structure D was taken as new starting point of step 2 (red dash line of Figure 3b). This intramolecular  $S_N2$  nucleophilic substitution was also easy via ts-Din3 with activation energy of 8.5 kcal mol<sup>-1</sup> by exothermic -18.1 kcal mol<sup>-1</sup> affording in3, from which the dearomatized ring closure product 7 was obtained after the release of Br<sup>-</sup>. The transition vector is typical corresponding to obvious nucleophilic attack from C3 to C1, concerted leaving of Br from C1 (2.1, 2.4 Å) and recovered C3-C4 to single (Figure 4h). Evidently intramolecular  $S_N2$  nucleophilic substitution is rate-limiting for spirocyclopropanation of 5-alkenylthiazolone more favorable than that of  $\pi$ -allylpalladium 1,4-dipole from kinetics.

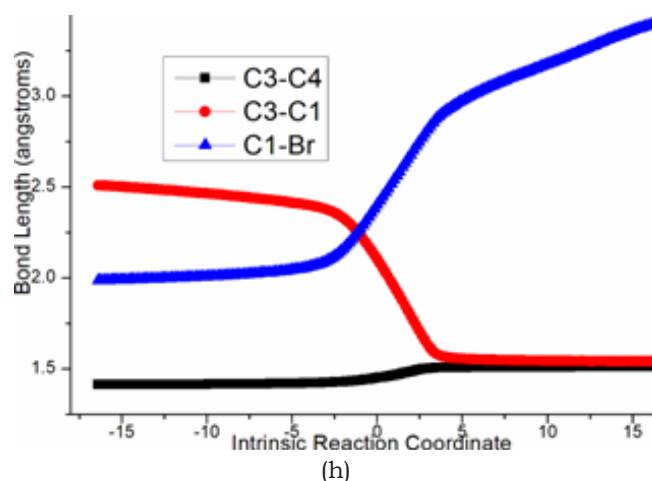


**Figure 4(h):** Evolution of bond lengths along the IRC for (h) ts-Din3 at B3LYP/6-311++G(d,p) level.

### Conclusion

Our DFT calculations provide the first theoretical investigation on Pd(0)-catalyzed spirocyclopropanation of  $\pi$ -allylpalladium 1,4-dipole with *gem*-difluoroalkene and 1,4-addition-induced dearomatization of 5-alkenylthiazolone with 2-bromomalonate. On one hand, the  $\pi$ -allylpalladium 1,4-zwitterionic species was afforded as stable five-membered ring by oxidative addition of methylenetriethylamine carbonate to Pd(0) and rate-limiting decarboxylation. Then via nucleophilic addition, the electrophilic



gem-difluorinated carbon was attacked by anionic oxygen forming zwitterionic intermediate with dual Pd- $\pi$  coordination. The intramolecular spirocyclization undergoes through attack of anionic carbon to central carbon of  $\pi$ -allylpalladium giving palladacyclobutane, of which the reductive elimination releases oxa/azaspiro[2.4]-heptane and regenerates Pd(0). The major Pd(0)-catalyzed spirocyclopropanation is prior to competitive  $\beta$ -F elimination.

On the other hand, carbanion was furnished for deprotonated bromomalonate. In the meantime, carbonyl of 5-alkenylthiazolone was activated by quaternary ammonium Me<sub>4</sub>N<sup>+</sup> with enhanced electrophilicity of C-C double bond, which was attacked by carbanion in Michael 1,4-addition forming aromatized enolate intermediate after removal of Me<sub>4</sub>N<sup>+</sup>. Subsequently, the rate-limiting intramolecular S<sub>N</sub>2 nucleophilic substitution took place affording dearomatized ring closure product spirocyclopropylthiazole and the release of Br<sup>-</sup>. The spirocyclopropanation of 5-alkenylthiazolone is more favorable than that of  $\pi$ -allylpalladium 1,4-dipole from kinetics. The positive solvation effect is suggested by decreased absolute and activation energies in solution compared with in gas. These results are supported by Multiwfn analysis on FMO composition of specific TSs, and MBO value of vital bonding, breaking.

## References

1. Sakla AP, Kansal P, Shankaraiah N (2021) Syntheses and applications of spirocyclopropyl oxindoles: A decade review. *Eur J Org Chem* 2021: 757-772.
2. Zhang GP, Huang S, Jiang YJ, Liu XY, Ding CH, et al. (2019) Pd-catalyzed enantioselective cyclopropanation of nitriles with mono substituted allyl carbonates enabled by the bulky n-heterocyclic carbene ligand. *Chem Commun* 55: 6449-6452.
3. Gao C, Zhang T, Li X, Wu JD, Liu J (2022) Asymmetric decarboxylative [3 + 2] cycloaddition for the diastereo- and enantioselective synthesis of spiro [2.4] heptanes via cyclopropanation. *Org Chem Front* 9: 2121-2128.
4. Trost BM, Jiao Z, Liu Y, Min C, Hung CIJ (2020) Palladium-catalyzed enantioselective cycloadditions of aliphatic 1,4-dipoles: access to chiral cyclohexanes and spiro [2.4] heptanes. *J Am Chem Soc* 142: 18628-18636.
5. Liu C, Zeng H, Zhu C, Jiang H (2020) Recent advances in three-component difunctionalization of gem-difluoroalkenes. *Chem Commun* 56: 10442-10452.
6. Liu C, Zhu C, Cai Y, Jiang H (2021) Solvent-switched oxidation selectivities with O<sub>2</sub>: controlled synthesis of  $\alpha$ -difluoro-(thio)methylated alcohols and ketones. *Angew Chem Int Ed* 60: 12038-12045.
7. Qi S, Gao S, Xie X, Yang J, Zhang J (2020) Palladium-catalyzed fluoroarylation of gem-difluoroalkynes to access trisubstituted trifluoromethyl allenes. *Org Lett* 22(13): 5229-5234.
8. Li J, Xu C, Wei N, Wang M (2017) Synthesis of 2,2-difluorinated 4-isoflavanols/4-thioisoflavanols via a base-catalyzed [4 + 2] annulation reaction of gem-difluoroolefins. *J Org Chem* 82: 11348-11357.
9. Liu J, Yu L, Zheng C, Zhao G (2021) Asymmetric synthesis of 2,2-difluorotetrahydrofurans through palladium-catalyzed formal [3+ 2] cycloaddition. *Angew Chem Int Ed* 60: 23641-23645.
10. Kamlar M, Urban M, Veselý J (2023) Enantioselective synthesis of spiro heterocyclic compounds using a combination of organocatalysis and transition-metal catalysis. *Chem Rec* 23: e202200284.
11. Müller G, Berkenbosch T, Benningshof J, Stumpfe D, Bajorath J (2017) Charting biologically relevant spirocyclic compound space. *Chem Eur J* 23: 703-710.
12. Patel DM, Patel PJ, Patel HM (2022) Catalytic stereoselective multicomponent reactions for the synthesis of spiro derivatives: recent progress. *Eur J Org Chem* 2022: e202201119.
13. Tanasova M, Sturla SJ (2021) Chemistry and biology of acylfulvenes: Sesquiterpene-derived antitumor agents. *Chem Rev* 112(6): 3578-3610.
14. Malloy KL, Choi H, Fiorilla C, Valeriote FA, Matainaho T, et al. (2012) Hoiamide D, a marine cyanobacteria-derived inhibitor of p53/MDM2 interaction. *Bioorg Med Chem Lett* 22: 683-688.
15. Song YX, Du DM (2019) Bifunctional squaramide-catalysed asymmetric michael/hemiketalization/retro-aldol reaction of unsaturated thiazolones with  $\alpha$ -nitroketones: Synthesis of chiral 4-acyloxythiazole derivatives. *Adv Synth Catal* 361: 1-9.
16. Ansari MF, Idrees D, Hassan Md I, Ahmad K, Avecilla F, et al. (2018) Design, synthesis and biological evaluation of novel pyridine-thiazolidinone derivatives as anticancer agents: Targeting human carbonic anhydrase IX. *Eur J Med Chem* 144: 544-556.
17. Yang KX, Ji DS, Zheng H, Gu Y, Xu PF (2022) Organocatalytic inverse-electron-demand Diels-Alder reaction between 5-alkenyl thiazolones and  $\beta,\gamma$ -unsaturated carbonyl compounds. *Chem Commun* 58: 4227-4230.
18. Mei MS, Wang YJ, Zhang GS, Tang JY, Tian P, et al. (2021) Catalyst-controlled diastereoselectivity switch in the asymmetric [3 + 2] annulation of isatin-derived MBH carbonates and 5-alkenylthiazol-4(5h)-ones. *Org Lett* 23: 7336-7341.
19. Fang QY, Yi MH, Wu XX, Zhao LM (2020) Regio- and diastereoselective spirocyclopropanation of benzofuran-derived azadienes through 1,4-addition-induced dearomatization reaction under mild conditions. *Org Lett* 22: 5266-5270.
20. Ye F, Ge Y, Spannenberg A, Neumann H, Beller M (2020) The role of allyl ammonium salts in palladium-catalyzed cascade reactions towards the synthesis of spiro-fused heterocycles. *Nat Commun* 11: 5383.
21. Yang L, Tao Z, Xu HD, Shen MH, Chu H (2024) Synthesis of gem-difluorinated oxa/azaspiro [2.4] heptanes via palladium-catalyzed spirocyclopropanation. *Org Lett* 27: 5782-5787.
22. Zhong C, Wang X, Li SJ, Tu MS, Zhang YC (2023) Base-promoted formal (2+1) cycloaddition of benzofuran-derived oxadienes with bromomalonates. *Synlett* 34: 1704-1708.
23. Carceller-Ferrer L, Blay G, Muñoz MC, Pedro JR, Vila C (2024) Diastereo- and enantioselective organocatalytic synthesis of spirocyclopropyl pyrazolones. *Adv Synth Catal* 366: 698-703.
24. Yang K, Jia A, Chen J, Tang Y, Liu S, et al. (2024) K<sub>2</sub>CO<sub>3</sub> promoted spirocyclopropanation of thiazole-derived oxadienes via 1,4-addition-induced dearomatization reaction. *Chemistry Select* 9: e202303859.
25. Frisch MJ, Trucks GW, Schlegel HB, et al. (2010) Gaussian 09 (Revision B.01), Gaussian, Inc., Wallingford, CT.
26. Hay PJ, Wadt WR (1985) Ab initio effective core potentials for molecular calculations-potentials for the transition-metal atoms Sc to Hg. *J Chem Phys* 82: 270-283.
27. Lv H, Han F, Wang N, Lu N, Song Z, et al. (2022) Ionic liquid catalyzed c-c bond formation for the synthesis of polysubstituted olefins. *Eur J Org Chem* 2022: e202201222.
28. Zhuang H, Lu N, Ji N, Han F, Miao C (2021) Bu<sub>4</sub>NHSO<sub>4</sub>-catalyzed direct n-allylation of pyrazole and its derivatives with allylic alcohols in water: A metal-free, recyclable and sustainable system. *Advanced Synthesis & Catalysis* 363: 5461-5472.
29. Lu N, Lan X, Miao C, Qian P (2020) Theoretical investigation on transformation of Cr(II) to Cr(V) complexes bearing tetra-NHC and group transfer reactivity. *Int J Quantum Chem* 120: e26340.
30. Lu N, Liang H, Qian P, Lan X, Miao C (2020) Theoretical investigation on the mechanism and enantioselectivity of organocatalytic asymmetric Povarov reactions of anilines and aldehydes. *Int J Quantum Chem* 120:



- e26574.
31. Lu N, Wang Y (2023) Alloy and media effects on the ethanol partial oxidation catalyzed by bimetallic Pt<sub>6</sub>M (M= Co, Ni, Cu, Zn, Ru, Rh, Pd, Sn, Re, Ir, and Pt). *Computational and Theoretical Chemistry* 1228: 114252.
32. Becke AD (1996) Density-functional thermochemistry. IV. A new dynamical correlation functional and implications for exact-exchange mixing. *J Chem Phys* 104: 1040-1046.
33. Lee CT, Yang WT, Parr RG (1988) Development of the colle-salvetti correlation-energy formula into a functional of the electron density. *Phys Rev B* 37(2): 785-789.
34. Catellani M, Mealli C, Motti E, Paoli P, Perez-Carrero E, et al. (2002) Palladium-arene interactions in catalytic intermediates: An experimental and theoretical investigation of the soft rearrangement between  $\eta^1$  and  $\eta^2$  coordination modes. *J Am Chem Soc* 124: 4336-4346.
35. Zicovich-Wilson CM, Pascale F, Roetti C, Saunders VR, Dovesi R (2004) Calculation of the vibration frequencies of  $\alpha$ -quartz: The effect of hamiltonian and basis set. *J Comput Chem* 25: 1873-1881.
36. Nielsen RJ, Goddard WA (2006) Mechanism of the aerobic oxidation of alcohols by palladium complexes of N-heterocyclic carbenes. *J Am Chem Soc* 128: 9651-9660.
37. Zandler ME, D'Souza F (2006) The remarkable ability of B3LYP/3-21G(\*) calculations to describe geometry, spectral and electrochemical properties of molecular and supramolecular porphyrin-fullerene conjugates. *Comptes Rendus Chimie* 9: 960-981.
38. Marenich AV, Cramer CJ, Truhlar DG (2009) Universal solvation model based on solute electron density and on a continuum model of the solvent defined by the bulk dielectric constant and atomic surface tensions. *J Phys Chem B* 113: 6378-6396.
39. Tapia O (1992) Solvent effect theories: Quantum and classical formalisms and their applications in chemistry and biochemistry. *J Math Chem* 10: 139-181.
40. Tomasi J, Persico M (1994) Molecular interactions in solution: an overview of methods based on continuous distributions of the solvent. *Chem Rev* 94: 2027-2094.
41. Tomasi J, Mennucci B, Cammi R (2005) Quantum mechanical continuum solvation models. *Chem Rev* 105: 2999-3093.
42. Reed AE, Weinstock RB, Weinhold F (1985) Natural population analysis. *J Chem Phys* 83: 735-746.
43. Reed AE, Curtiss LA, Weinhold F (1988) Intermolecular interactions from a natural bond orbital donor-acceptor viewpoint. *Chem Rev* 88: 899-926.
44. Lu T, Chen F (2012) Multiwfn: A multifunctional wavefunction analyzer. *J Comput Chem* 33: 580-592.